

1 **Title: Semaphorin4D induces inhibitory synapse formation by rapid**
2 **stabilization of presynaptic boutons via MET co-activation**

3

4 **Abbreviated title:** Sema4D induces inhibitory bouton stabilization via MET

5

6 **Authors:** Cátia P. Frias¹, Tom Bresser¹, Lisa Scheefhals¹, Hai Yin Hu¹, Paul M. P. van
7 Bergen en Henegouwen¹, Casper C. Hoogenraad¹ and Corette J. Wierenga^{1*}

8

9 **Affiliation:** ¹Cell Biology, Department of Biology, Faculty of Science, Utrecht University,
10 3584 CH Utrecht, the Netherlands

11

12 ***Corresponding author:**

13 Corette J. Wierenga

14 Utrecht University

15 Department of Biology, Faculty of Science

16 Padualaan 8, 3584CH Utrecht

17 The Netherlands

18 E-mail: c.j.wierenga@uu.nl

19 Tel. +31-30-253 2659

20

21

22 Number of pages: 28
23 Number of figures: 9
24 Number of tables: 0
25 Number of words in the abstract: 238 (max 250)
26 Number of words in the introduction: 605 (max 650)
27 Number of words in the discussion: 1492 (max 1500)

28

29

30 **Acknowledgements:**

31 We would like to thank G. Szábo for kindly providing the GAD65-GFP mice, R. van Dorland
32 for technical support, M. van Kesteren for analysis of LatB immunodata, S. Paradis for
33 helpful comments and scientific discussions and A. Akhmanova, G.G. Turrigiano and R.J.
34 Pasterkamp for critically reading the manuscript. This work was supported by the People
35 Programme (Marie Curie Actions) of the European Union's Seventh Framework Programme
36 FP7/2007-2013/ under REA grant agreement 289581 (C.P.F.), a Marie Curie Reintegration
37 Grant 256284 (C.J.W.) and the Netherlands Organization for Scientific Research (NWO-
38 VIDI, C.J.W., NWO-VICI, C.C.H.).

39

40

41 **Conflict of Interest:**

42 The authors declare no competing financial interests.

43 **ABSTRACT**

44 Changes in inhibitory connections are essential for experience-dependent circuit adaptations.
45 Defects in inhibitory synapses are linked to neurodevelopmental disorders, but the molecular
46 processes underlying inhibitory synapse formation are not well understood. Here we use high
47 resolution two-photon microscopy in organotypic hippocampal slices to examine the signaling
48 pathways induced by the postsynaptic signaling molecule Semaphorin4D (Sema4D) during
49 inhibitory synapse formation. By monitoring changes in individual GFP-labeled presynaptic
50 boutons we found that the primary action of Sema4D is to induce stabilization of presynaptic
51 boutons within tens of minutes. Stabilizing boutons rapidly recruited synaptic vesicles, which
52 was followed by accumulation of postsynaptic gephyrin. Newly formed inhibitory synapses
53 were complete and functional after 24 hours, as determined by electrophysiology and
54 immunohistochemistry. We further showed that Sema4D signaling is regulated by network
55 activity and can induce a local increase in bouton density, suggesting a possible role in circuit
56 adaptation. We further examined the intracellular signaling cascade triggered by Sema4D and
57 found that bouton stabilization occurred through rapid remodeling of actin, and this could be
58 mimicked by the actin-depolymerizing drug Latrunculin B or by reducing ROCK activity.
59 The intracellular signaling cascade required activation of the receptor tyrosine kinase MET,
60 which is a well-known autism risk factor. Our immunohistochemistry data suggests that MET
61 may be localized to presynaptic inhibitory axons. Together, our data yield important insights
62 in the molecular pathway underlying activity-dependent Sema4D-induced synapse formation
63 and reveal a novel role for MET in inhibitory synapses.

64

65

66 **Significance Statement**

67 GABAergic synapses provide the main inhibitory control of neuronal activity in the brain. We
68 make important steps in unraveling the molecular processes that take place when formation of
69 inhibitory synapses is triggered by a specific signaling molecule, Sema4D. We find that this
70 process depends on network activity and involves specific remodeling of the intracellular
71 actin cytoskeleton. We also reveal a previously unknown role for MET in inhibitory synapses.
72 As defects in GABAergic synapses have been implied in many brain disorders, and mutations
73 in MET are strong risk factors for autism, our findings urge for a further investigation of the
74 role of MET at inhibitory synapses.

75

76 INTRODUCTION

77

78 GABAergic synapses provide the main inhibitory control over neuronal activity in the brain
79 and are indispensable for shaping network function (Isaacson and Scanziani, 2011). In
80 postnatal brain tissue, in which the majority of inhibitory connections have been established,
81 synapse formation and disassembly is still ongoing (Caroni et al., 2012). Formation and
82 disassembly of inhibitory synapses in the brain play an important role in experience-
83 dependent circuit adaptation (Hensch, 2005; Keck et al., 2011; Chen et al., 2015; Froemke,
84 2015; Sprekeler, 2017) and defects in GABAergic synapses have been observed in many
85 neurodevelopmental disorders (Marín, 2012; Cellot and Cherubini, 2014; Nelson and Valakh,
86 2015). We and others have previously shown that inhibitory axons are dynamic structures
87 with boutons forming and disappearing with apparently stochastic dynamics (Fu and Huang,
88 2010; Dobie and Craig, 2011; Kuriu et al., 2012; Frias and Wierenga, 2013). These ongoing
89 bouton dynamics allow quick updating of connections in response to changes in the neuronal
90 circuitry (Staras, 2007; Frias and Wierenga, 2013). New inhibitory synapses form by the
91 emergence of new presynaptic boutons at pre-existing axon-dendrite crossings (Wierenga et
92 al., 2008; Schuemann et al., 2013). However, the signaling pathways that regulate the multiple
93 steps during inhibitory synapse formation are not well understood (Wierenga, 2017).

94 In the recent years, enormous progress has been made by the identification and
95 characterization of proteins that are involved in the formation of inhibitory synapses (Siddiqui
96 and Craig, 2011; Krueger-Burg et al., 2017; Lu et al., 2017). The class 4 semaphorin Sema4D,
97 originally identified as an axon guidance factor (Kolodkin et al., 1993; Pasterkamp, 2012), has
98 been shown to play a crucial role in this process. Formation of GABAergic synapses was
99 shown to depend on Sema4D signaling, as knockdown of postsynaptic Sema4D led to a 30%
100 reduction of GABAergic synapses in primary cultures (Paradis et al., 2007). In addition, acute
101 activation of Sema4D pathway by adding a soluble form of the extracellular part of Sema4D
102 to primary hippocampal cultures induces rapid increase of GABAergic synapses (Kuzirian et
103 al., 2013; Raissi et al., 2013). The observation that somatic and dendritic synapses responded
104 equally to Sema4D signaling (Kuzirian et al., 2013) suggests that Sema4D could be acting on
105 a broad range of (or perhaps all) inhibitory synapses.

106 Despite its well-characterized physiological importance, relatively little is known about the
107 cellular mechanism by which Sema4D induces inhibitory synapse formation. It was shown
108 that Sema4D acts as a postsynaptic protein and requires its receptor PlexinB1 to induce

109 inhibitory synapses (Kuzirian et al., 2013; Raissi et al., 2013). The signal cascades that are
110 triggered by Semaphorin4D-PlexinB1 interaction have been well studied in other cells and these
111 studies revealed that Semaphorin4D action is highly cell-specific (Zhou et al., 2008; Cagnoni and
112 Tamagnone, 2014). For instance, Semaphorin4D has been reported to either suppress or enhance
113 cellular adhesion and/or migration, depending on the cell type (Oinuma et al., 2006; Basile et
114 al., 2007; Giacobini et al., 2008; Swiercz et al., 2008). The intracellular molecular events
115 downstream of Semaphorin4D/PlexinB1 signaling that lead to inhibitory synapse induction are
116 currently not known.

117 In the current study, we used high resolution two-photon microscopy in organotypic
118 hippocampal slices to characterize Semaphorin4D regulation of inhibitory synapse formation in
119 intact tissue and to examine the underlying molecular pathway. We found that Semaphorin4D
120 signaling specifically regulates the rapid stabilization of inhibitory boutons along the axon
121 and that local bouton stabilization by Semaphorin4D can result in local changes in bouton density
122 within tens of minutes. These rapid presynaptic changes are followed by subsequent
123 recruitment of pre- and postsynaptic proteins to complete the formation of functional
124 inhibitory synapses over the course of the next hours. We also found that Semaphorin4D-induced
125 bouton stabilization is activity-dependent. The intracellular pathway for bouton stabilization
126 involves specific remodeling of the actin cytoskeleton, and requires the activation of the
127 receptor tyrosine kinase MET. Our data unravel an important regulatory pathway of activity-
128 dependent inhibitory synapse formation and reveal a novel role for the receptor tyrosine
129 kinase MET in Semaphorin4D-induced formation of inhibitory synapses.

130 **EXPERIMENTAL PROCEDURES**

131

132 **Animals**

133 All animal experiments were performed in compliance with the guidelines for the welfare of
134 experimental animals issued by the Federal Government of The Netherlands. All animal
135 experiments were approved by the Animal Ethical Review Committee (DEC) of Utrecht
136 University.

137

138 **Hippocampal slice cultures**

139 Hippocampal slice cultures (400 μm thick) were prepared from postnatal day 5-7 of both male
140 and female GAD65-GFP mice (López-Bendito et al., 2004) as previously described (Müllner
141 et al., 2015). In short, the hippocampi were dissected in ice-cold HEPES-GBSS (containing
142 1.5 mM $\text{CaCl}_2 \cdot 2\text{H}_2\text{O}$, 0.2 mM KH_2PO_4 , 0.3 mM $\text{MgSO}_4 \cdot 7\text{H}_2\text{O}$, 5 mM KCl, 1 mM
143 $\text{MgCl}_2 \cdot 6\text{H}_2\text{O}$, 137 mM NaCl, 0.85 mM Na_2HPO_4 and 12.5 mM HEPES) supplemented with 1
144 mM kynurenic acid and 25 mM glucose, and plated in a MEM-based medium (MEM
145 supplemented with 25 % HBSS, 25 % horse serum, 30 mM glucose and 12.5 mM HEPES).

146 In GAD65-GFP mice, approximately 20% of the CA1 interneurons express GFP from early
147 embryonic developmental stage into adulthood (López-Bendito et al., 2004; Wierenga et al.,
148 2010). The majority of GFP-labeled interneurons expresses reelin and VIP, while
149 parvalbumin and somatostatin expression is nearly absent (Wierenga et al., 2010). For our
150 study, the relatively low number of GFP-positive axons is crucial for proper analysis of
151 individual boutons.

152 The slices were kept in culture for at least one week before the experiments (range 7-21 days
153 *in vitro*) at 35 °C in 5 % CO_2 . For live imaging experiments, slices were transferred to an
154 imaging chamber, where they were continuously perfused with carbogenated artificial
155 cerebrospinal fluid (ACSF; containing 126 mM NaCl, 3 mM KCl, 2.5 mM CaCl_2 , 1.3 mM
156 MgCl_2 , 1.25 mM NaH_2PO_4 , 26 mM NaHCO_3 , 20 mM glucose and 1mM Trolox). The
157 temperature of the chamber was maintained at 37°C. Treatment and control experiments were
158 conducted in slices from sister cultures.

159

160 **Pharmacological treatments**

161 The following drugs were used: 0.1/0.2 % DMSO, 1 nM Fc and Sema4D-Fc (amino acids 24-
162 711) (both R&D Systems), 100 nM Latrunculin B (Santa Cruz Biotechnology), 200 nM

163 Jaspalakinolide (Tocris Bioscience), 1 μ M PHA-665752 (Sigma-Aldrich) and 10 μ M Y-27632
164 (Sigma-Aldrich). We used the small molecule PHA-665752 (PHA), a highly specific MET
165 inhibitor (Christensen et al., 2003; Deguchi et al., 2016), to decrease endogenous
166 phosphorylation of MET, without affecting MET expression or neuronal cell viability. We
167 used 10 nM Fc or Sema4D for the local puffing experiments.
168 For treatments that were followed by immunostaining of inhibitory synapses, 1 nM Fc or
169 Sema4D-Fc was added to the culturing medium and slices were left in the incubator for 2, 6
170 or 24 h before fixation.

171

172 **Two-photon imaging**

173 For acute treatments, drugs were added to the perfusion ACSF after a baseline period of 40
174 minutes (5 time points) and we continued imaging for an additional 10 time points in the
175 wash-in period (total imaging period is 140 minutes). In longer treatments, we treated the
176 slices for 6 hours after the baseline period (5 imaging time points) at the microscope and
177 restarted imaging for 5 time points, for a total treatment period of 6 hours and 40 minutes
178 (400 minutes). For activity blockade, 0.5 μ M tetrodotoxin citrate (TTX; Tocris Bioscience)
179 was added to the perfusion ACSF prior to the transfer of the slice to the imaging chamber.
180 Time-lapse two-photon microscopy images were acquired on a Femtonics 2D two-photon
181 laser-scanning microscope (Budapest, Hungary), with a Nikon CFI Apochromat 60X NIR
182 water-immersion objective. GFP was excited using a laser beam tuned to 910 nm (Mai Tai
183 HP, Spectra Physics). The 3D images (93.5 μ m x 93.5 μ m in xy, 1124 x 1124 pixels)
184 consisted of 29-33 z stacks (0.5 μ m step size in z). Small misalignments due to drift were
185 manually compensated during the acquisition.

186 For the local treatment, we used HEPES-ACSF (containing 126 mM NaCl, 3 mM KCl, 2.5
187 mM CaCl₂, 1.3 mM MgCl₂, 1.25 mM NaH₂PO₄, 20 mM glucose, and 10 mM HEPES; pH
188 7.41) with 20 μ M Alexa 568 (Invitrogen), in order to visualize the spread of the local puff.
189 Sema4D or Fc was added to the HEPES-ACSF to a final concentration of 10 nM. The
190 solution was loaded into a patch pipette (4-6 M Ω), and was locally applied to a GFP-
191 labeled axon using a Picospritzer II (General Valve). Time-lapse two photon microscopy
192 imaging was performed as described previously, except that a second laser (Spectra Physics)
193 was used at 840 nm to visualize the area of the puff. The 3D images (51.3 μ m x 51.3 μ m in
194 xy, 620 x 620 pixels) consisted of 18-22 z stacks (0.5 μ m step size in z). After a baseline
195 period of 20 minutes (5 TPs), the pipette was put into position before the stimulation. The
196 stimulation consisted of 300 puffs of 20-50 ms at 2 Hz. The pipette was carefully retracted

197 before continuing the time series for 10 additional time points (total imaging period of 70
198 minutes).

199

200 **Two-photon image analysis**

201 The analysis of inhibitory bouton dynamics was performed semi-automatically using ImageJ
202 (US National Institute of Health) and Matlab-based software (Mathworks). The 3D
203 coordinates of individual axons were selected at every time point by using the CellCounter
204 plugin (Kurt De Vos, University of Sheffield, Academic Neurology). For each image, 1-5
205 stretches of axons (average length 78 μm with standard deviation 18 μm , with average of 31
206 boutons per axon with standard deviation 11; for local treatment experiments, average length
207 39 μm with standard deviation 8 μm , with average of 14 boutons per axon with standard
208 deviation of 4) were selected for analysis.

209 A 3D intensity profile along the selected axons was constructed at each time point, and
210 individual boutons were identified in a two-step process using custom-made Matlab software
211 (Schuemann et al., 2013). In brief, an axon threshold was calculated to differentiate the axon
212 from the background (2 standard deviations above mean intensity); subsequently, a local
213 threshold (0.5 standard deviation above mean axon intensity) identified the boutons along the
214 selected axon. Only boutons with at least 5 pixels above bouton threshold were included.
215 Each image stack was visually examined, and false positives and negatives were corrected
216 manually. Only raw data was analyzed; images were median-filtered for illustration purposes
217 only.

218 Boutons were classified as persistent when they were present during all time points, and non-
219 persistent when they were absent during one or more time points during the imaging session.
220 The average fraction of persistent and non-persistent boutons was calculated by normalization
221 to the average number of boutons per axon. To bias our analysis towards synaptic events
222 (Schuemann et al., 2013), we restricted our analysis to boutons that appeared for at least 2
223 time points at the same location during the imaging period. We verified that our main
224 conclusions did not change when this restriction was released. Based on their presence during
225 baseline and treatment periods, we defined five subgroups of non-persistent boutons: new
226 boutons (not present during baseline), lost boutons (not present during wash-in), stabilizing
227 boutons (non-persistent during baseline, persistent during wash-in), destabilizing boutons
228 (persistent during baseline, non-persistent during wash-in), and transient boutons (non-
229 persistent in baseline and wash-in) (Fig. 1). Average fraction of each subgroup of boutons was
230 normalized to the total average number of non-persistent (NP) boutons per axon. The duration

231 of each bouton was defined as the number of time points present divided by the total number
232 of time points per period. Bouton density was calculated as the average number of boutons at
233 all time points divided by the 3D axon length.

234

235 **Electrophysiology**

236 During the experiment, the slice was placed in a recording chamber perfused with oxygenated
237 artificial cerebral spinal fluid (ACSF) at a rate of 1 ml/min. The recording ACSF consisted of
238 126 mM NaCl, 3 mM KCl, 2.5 mM CaCl₂, 1.3 mM MgCl₂, 1.25 mM Na₂H₂PO₄, 26 mM
239 NaHCO₃, and 20 mM glucose. Whole cell voltage clamp recordings were performed at 35 °C
240 in CA1 cells of GAD65-GFP slice cultures at DIV 13-19. Recordings were made on a
241 Multiclamp 700B amplifier (Molecular Devices) and stored using pClamp 10 software. To
242 isolate sIPSCs, 20 μM DNQX and 50 μM APV were added to the recording ACSF. For
243 mIPSCs, 0.5 μM TTX was added as well. Thick walled borosilicate pipettes of 3-6 MΩ were
244 filled with an internal solution containing 70 mM K-gluconate, 70 mM KCl, 0.5 mM EGTA,
245 10 mM HEPES, 4 mM MgATP, 0.4 mM NaGTP, and 4 mM Na₂Phosphocreatine. Cells were
246 excluded from analysis if the series resistance increased more than 35 %. IPSCs were
247 automatically detected in Clampfit and further analyzed in custom Matlab scripts. Detected
248 events within 3 ms of each other were merged and events smaller than 3 times the RMS of the
249 signal were excluded. The cumulative distributions for individual experiments were
250 interpolated to generate the average distribution.

251

252 **Immunohistochemistry, confocal imaging and image analysis**

253 For *post hoc* immunohistochemistry, organotypic hippocampal slices were fixed in 4 % (w/v)
254 paraformaldehyde for 30 minutes at room temperature. Slices were rinsed in phosphate buffer
255 and permeabilized with 0.5 % TritonX-100 in phosphate buffer for 15 minutes. Slices were
256 blocked with 0.2 % TritonX-100, 10 % goat serum (ab7481, Abcam) in phosphate buffer for
257 60 minutes. Primary antibodies were applied overnight at 4°C in blocking solution. After
258 washing, slices were incubated with secondary antibodies in blocking solution for 4h at room
259 temperature. Slices were washed and mounted on slides in Vectashield mounting medium
260 (Vector Labs).

261 The following primary and secondary antibodies were used: rabbit α-VGAT (1:1000;
262 Synaptic Systems, 131 003), mouse α-gephyrin (1:1000; Synaptic Systems, 147 011), guinea
263 pig α-VGLUT (1:400; Millipore, AB5905), rabbit α-Homer (1:1000; Synaptic Systems, 160
264 002), mouse α-myc (1:100; Oncogene Research Products, OP10), mouse α-MET (1:500;

265 Santa Cruz Biotechnology, sc-8057), Alexa405-, Alexa-488 and Alexa-568 conjugated
266 secondary antibodies (Invitrogen). For staining MET we used a previously described myc-
267 tagged nanobody, which was shown to recognize MET with low nanomolar affinity (Heukers
268 et al., 2014). We visualized the nanobody with an antibody against the C-terminal myc tag.
269 We validated the nanobody staining in primary hippocampal cultures using a previously
270 described immunostaining protocol (Esteves da Silva et al., 2015).

271 For immunostainings, high resolution confocal laser scanning microscopy was performed on a
272 Zeiss LSM-700 system with a Plan-Apochromat 63x 1.4 NA oil immersion objective. Each
273 image was a z-series of 11-35 images (0.3 μm z step size), each averaged 4 times. The
274 imaging area in the CA1 region was 78 x 78 μm (1024 x 1024 pixels). The confocal settings
275 were kept the same to compare fluorescence intensities between slices.

276 For the quantification of VGAT and gephyrin intensities per image, we determined per image
277 the mean intensity of 3 randomly chosen areas of 10 x 10 μm of the average projection image
278 from the 5 middle z-layers. For the cumulative plots individual values (per area) were used.
279 Synaptic puncta size and number were determined using the PunctaAnalyzer plugin, and
280 inhibitory synapses were defined as overlapping VGAT and gephyrin puncta. For determining
281 co-localization of GFP-labeled boutons with synaptic marker VGAT or with MET, we
282 manually inspected individual boutons through all z-sections. A bouton was only considered
283 positive when at least one z stack of the bouton overlapped with VGAT or MET staining. The
284 images were median-filtered only for illustration purposes.

285

286 **Statistical Analysis**

287 Data are represented as mean values \pm standard error of the mean, unless stated otherwise.
288 Statistical analysis was performed using GraphPad Prism software. Results from treatment
289 and control experiments were compared using the Mann-Whitney U test (MW). The Chi-
290 Square test (χ^2) was used for comparing the fraction of axons with/without stabilizing
291 boutons. For comparing multiple groups, we used the Kruskal-Wallis test (KW) followed by a
292 posthoc Dunn's comparison test. We used a One-Way ANOVA followed by a Dunnett's
293 multiple comparison test (One-Way ANOVA) to compare the effect of wash-in of PHA over
294 time. We used a Two-Way ANOVA followed by a Sidak's multiple comparisons test (Two-
295 Way ANOVA) to compare treatment effects at multiple time points. For the comparison of
296 cumulative distributions, we used the Kolmogorov-Smirnov (KS) test. We have indicated the
297 tests and p-values in the figure legends. Differences between control and treatment were
298 considered significant when $p < 0.05$ (*, $p < 0.05$; **, $p < 0.01$; ***, $p < 0.001$). In all figure

299 legends and text, N indicates the number of independent experiments, and n indicates the
300 number of axons/images analyzed.

301 **RESULTS**

302

303 We performed time-lapse two-photon microscopy in organotypic hippocampal cultures from
304 GAD65-GFP mice to monitor the dynamics of inhibitory boutons in the CA1 region of the
305 hippocampus (Wierenga et al., 2008; Schuemann et al., 2013). In GAD65-GFP mice,
306 approximately 20% of the CA1 interneurons express GFP. The majority of GFP-labeled
307 interneurons express reelin and VIP, while parvalbumin and somatostatin expression is nearly
308 absent (López-Bendito et al., 2004; Wierenga et al., 2010). High-resolution image stacks of
309 GFP-labeled inhibitory axons were acquired every 10 minutes, for a total period of 150
310 minutes (15 time points). Inhibitory boutons were remarkably dynamic and many boutons
311 appear, disappeared and reappeared during the course of the imaging period. To bias our
312 analysis towards synaptic events, we only included boutons that appeared for at least 2 time
313 points at the same location during the imaging period. We distinguished two main classes of
314 boutons: persistent boutons, which were present during all time points, and non-persistent
315 boutons, which were absent during one or more time points during the imaging session (Fig.
316 1A,B). Approximately 77 % (with standard deviation of 12 %) of inhibitory boutons at any
317 given time point were persistent (Fig. 1C), and they reflect inhibitory synapses (Wierenga et
318 al., 2008; Müllner et al., 2015). Non-persistent boutons reflect locations where inhibitory
319 synapses are ‘in transition’, e.g. where synapses are being formed or disassembled (Wierenga
320 et al., 2008; Dobie and Craig, 2011; Fu et al., 2012; Schuemann et al., 2013). Based on the
321 presence or absence of non-persistent boutons during a baseline and wash-in period (details
322 are given in the methods section), we distinguished 5 subgroups of non-persistent boutons:
323 new (N; absent during baseline), lost (L; absent during wash-in), stabilizing (S; non-persistent
324 during baseline, persistent during wash-in), destabilizing (D; persistent during baseline, non-
325 persistent during wash-in) and transient (non-persistent in both periods). These different
326 subgroups of non-persistent boutons not only differed in their incidence and duration (Fig.
327 1C,D), but also in their molecular composition, as assessed by immunostaining for the
328 presynaptic vesicular GABA transporter (VGAT) and the postsynaptic scaffold gephyrin (Fig.
329 1E). Stabilizing boutons, which were present for at least 90 minutes before fixation, showed
330 similar association with VGAT and gephyrin as persistent boutons, indicating that they are
331 nascent inhibitory synapses that have started to recruit pre- and postsynaptic proteins within
332 this period. Newly formed boutons, which were present for a short period before fixation,
333 showed a lower percentage of VGAT and gephyrin association. Boutons with longer total

334 lifetime before fixation showed higher association with VGAT and gephyrin, suggesting a
335 gradual recruitment of proteins over the imaging period (Fig. 1F). Recruitment of gephyrin
336 appeared delayed compared to VGAT, as previously reported (Wierenga et al., 2008; Dobie
337 and Craig, 2011). These data demonstrate that inhibitory presynaptic boutons are dynamic
338 structures that are continuously being formed and disassembled along the axons, and suggest
339 that non-persistent boutons reflect boutons at different stages of inhibitory synapse assembly
340 and disassembly.

341

342 **Inhibitory bouton stabilization during treatment with Sema4D**

343 It was recently shown that class 4 semaphorin Sema4D can rapidly induce an increase of
344 functional inhibitory synapses in hippocampal dissociated cultures (Kuzirian et al., 2013).
345 However, these data could not resolve if Sema4D directly promotes synapse formation or
346 rather prevents ongoing synapse elimination, thereby indirectly increasing synaptic density.
347 To examine the effect of Sema4D on ongoing inhibitory bouton dynamics, we bath applied
348 the extracellular domain of mouse Sema4D conjugated to the Fc region of mouse IgG2A
349 (Sema4D; 1 nM) and compared inhibitory bouton dynamics during a baseline period of 5 time
350 points and during Sema4D treatment in the subsequent 10 time points (Fig. 2A). We used Fc
351 alone (1 nM) as a control treatment (Kuzirian et al., 2013). Bath application of Sema4D did
352 not affect overall axonal morphology (Fig. 2A) and did not change the density of inhibitory
353 boutons (Fig. 2B). However, when we analyzed the different subgroups of non-persistent
354 boutons, we found that Sema4D treatment specifically enhanced the fraction of stabilizing
355 boutons from $6 \pm 2\%$ to $16 \pm 3\%$ (Fig. 2C). Indeed, this effect was also clear when we
356 analyzed the absolute density of boutons. The density of stabilizing boutons was increased by
357 >2 -fold, while other subgroups of boutons were unaffected (Fig. 2D-H). To examine how
358 Sema4D-induced stabilization developed over time, we quantified the number of boutons that
359 were present for 5 consecutive time points during the baseline and the wash-in period. We
360 found that Sema4D induced a marked increase in these boutons over the course of the wash-in
361 period (% stabilization, Fig. 2I), and strongly enhanced the number of boutons that had
362 stabilized at the end of this period (last 5 time points; Fig. 2J). Stabilizing boutons are
363 relatively rare in our slices, as under control conditions only 40% of the axons display one or
364 more stabilizing boutons. Treatment with Sema4D significantly increased this fraction to 77%
365 (Fig. 2K). Altogether, these data show that Sema4D treatment in intact tissue specifically
366 promotes the stabilization of inhibitory boutons within tens of minutes, without affecting
367 synapse elimination.

368

369 **Sema4D-induced stabilization of inhibitory boutons is the first step of inhibitory synapse**
370 **formation**

371 We next assessed whether Sema4D-induced bouton stabilization also results in an increase of
372 inhibitory synapses in our slices. We first examined if longer Sema4D treatment could
373 enhance the bouton stabilization effect. We compared dynamics of individual boutons during
374 baseline and after 6 h treatment (400 minutes total treatment) and found that longer Sema4D
375 treatment also induced prominent bouton stabilization, measured as fraction as well as
376 absolute density (Fig. 3A,B). However, the 6 h treatment did not increase bouton stabilization
377 beyond the 2 h level (Fig. 3C), suggesting that only a limited number of inhibitory boutons
378 can be stabilized by Sema4D treatment, resulting in saturation of the treatment effect already
379 after 2 hr. In addition to promoting bouton stabilization, with longer treatments we also
380 detected a small reduction in the fraction of transient boutons (Fig. 3A). This effect was only
381 revealed by analyzing the changes in density over time (Fig. 3D), which suggest that this may
382 reflect an indirect effect of prolonged bouton stabilization. These results indicate that the
383 Sema4D-induced stabilization of inhibitory boutons persists, but does not further increase,
384 with longer treatments.

385 We next asked if Sema4D-induced inhibitory bouton stabilization leads to the formation of
386 functional synapses. We treated organotypic hippocampal slices with 1 nM Fc or 1 nM
387 Sema4D for 24 h, and determined overall inhibitory synapse density by
388 immunohistochemistry. We used antibodies against presynaptic VGAT and postsynaptic
389 gephyrin to visualize inhibitory synapses (Fig. 3E,F). Sema4D induced a clear 24 ± 7 %
390 increase in the density of inhibitory synapses (Fig. 3G), suggesting that the observed
391 Sema4D-induced bouton stabilization after 2 h resulted in the formation of new synapses after
392 24 h. We used electrophysiological recordings to verify that these synapses were functional.
393 In agreement with the immunohistochemistry results, we found that 24 h treatment with
394 Sema4D increased the frequency of miniature inhibitory postsynaptic currents (mIPSCs) by
395 37 % (from 5.2 ± 0.5 to 7.1 ± 0.5 Hz), while mIPSC amplitude was not affected (Fig. 3H-K).
396 To determine the time course of the recruitment of pre- and postsynaptic elements during
397 synapse formation, we quantified VGAT and gephyrin immunostaining after 2, 6 and 24 h
398 treatments. Treatment with Sema4D induced an increase in the area of VGAT puncta, without
399 affecting their density (Fig. 4A-C). For gephyrin, Sema4D treatment caused an increase in
400 puncta density, but not in their size (Fig. 4D-F). The average puncta intensity was not affected
401 (at 24 h, VGAT: 107 ± 4 % of control, $p = 0.35$ (MW); gephyrin: 106 ± 5 % of control, $p =$

402 0.51 (MW)). Interestingly, the time course for presynaptic and postsynaptic changes was
403 different. Whereas an increase in presynaptic VGAT area could already be detected after 6 h,
404 the increase in postsynaptic gephyrin density was only evident after 24 h. These data are
405 consistent with gradual increase in presynaptic vesicle content and subsequent acquisition of
406 postsynaptic scaffolds at newly formed inhibitory synapses (Wierenga et al., 2008; Dobie and
407 Craig, 2011). Together, these data indicate that the initial Semaphorin 4D-induced stabilization of
408 inhibitory boutons is followed by a slower maturation process, resulting in an overall increase
409 in functional inhibitory synapses after Semaphorin 4D treatment.

410

411 **Semaphorin 4D-induced bouton stabilization relies on network activity**

412 We previously showed that inhibitory bouton dynamics are regulated by neuronal activity
413 (Schuemann et al., 2013). We therefore asked whether Semaphorin 4D-induced stabilization of
414 inhibitory boutons depended on network activity. Blocking activity by bath application of
415 tetrodotoxin (TTX) slightly decreased overall bouton dynamics in our slices (data not shown),
416 which is in accordance with our previous findings (Schuemann et al., 2013). However, we
417 found that in the presence of TTX Semaphorin 4D treatment no longer induced stabilization of
418 inhibitory boutons, and that Semaphorin 4D treatment even led to a reduction in bouton stabilization
419 compared to control (Fig. 5A,B). Indeed, whereas under control conditions Semaphorin 4D treatment
420 increased the number of axons that displayed stabilizing boutons, it led to a decrease in the
421 presence of TTX (Fig. 5C,D). These findings demonstrate that Semaphorin 4D treatment affects
422 bouton dynamics in an activity-dependent manner, and indicate that Semaphorin 4D promotes the
423 stabilization of inhibitory presynaptic boutons only in active neuronal networks.

424

425 **Local Semaphorin 4D-induced bouton stabilization**

426 Under physiological circumstances, Semaphorin 4D is a membrane-attached protein acting locally
427 (Pasterkamp, 2012; Raissi et al., 2013). Presynaptic boutons along the same axon interact and
428 share presynaptic proteins and vesicles (Staras, 2007; Bury and Sabo, 2016) and we wondered
429 if local Semaphorin 4D signaling would act differently compared to ubiquitous activation of Semaphorin 4D
430 signaling during bath application. We therefore locally applied Semaphorin 4D to short stretches
431 (~40 μm) of inhibitory axons (Fig. 5E). Local application with control solution appeared to
432 slightly reduce local bouton stabilization (compare control curves in 5F and 2I), possibly from
433 mechanical pressure. In contrast, local application of Semaphorin 4D induced robust stabilization of
434 inhibitory boutons in these axons (Fig. 5F), resulting in a significant increase in local bouton
435 density in these short axon stretches (Fig. 5G). This indicates that local application of

436 Sema4D is more potent to induce axonal changes than bath application, which failed to induce
437 a change in overall bouton density (compare Fig. 2B). This suggests that stabilizing boutons
438 may compete for presynaptic components within individual axons when Sema4D is bath
439 applied, limiting overall bouton density. Together, our results demonstrate that Sema4D-
440 signaling is capable to mediate rapid changes in local bouton density of inhibitory axons in an
441 activity-dependent manner.

442

443 **Actin remodeling by low doses of LatrunculinB promotes stabilization of inhibitory** 444 **boutons**

445 The Sema4D effect on inhibitory synapses was previously shown to be dependent on its
446 receptor PlexinB1 (Kuzirian et al., 2013). Sema4D/PlexinB1 signaling induces changes in the
447 intracellular actin cytoskeleton via multiple small GTPase signaling pathways in many
448 different cell types (Zhou et al., 2008; Cagnoni and Tamagnone, 2014). Some of these
449 downstream signaling pathways, which can modify actin in multiple ways, are mediated by
450 receptor tyrosine kinases, such as MET and ErbB-2, acting as co-receptors for PlexinB1. It
451 was shown in breast carcinoma cells that, when MET is co-activated, Sema4D/PlexinB1
452 signaling reduces RhoA levels and this results in actin depolymerization, while co-activation
453 of ErbB-2 leads, via RhoA activation, to actin polymerization (Swiercz et al., 2008; Sun et al.,
454 2012). To examine how the actin cytoskeleton is involved in inhibitory bouton dynamics, we
455 studied the effect of two actin remodeling drugs in our system with intended opposite effects:
456 the actin monomer sequestering drug LatrunculinB (LatB), which is generally considered an
457 actin depolymerizing drug, and the actin filament stabilizer Jasplakinolide (Jasp), which
458 promotes actin polymerization. In the low concentrations that we use here (100 nM LatB and
459 200 nM Jasp) these drugs perturb the actin cytoskeleton without affecting synaptic function
460 (Honkura et al., 2008; Rex et al., 2009). None of the treatments changed overall axon
461 morphology (Fig. 6A). We found that the fraction of stabilizing boutons was increased in the
462 presence of LatB, but not in the presence of Jasp (Fig. 6B,C). The effect of LatB seemed
463 highly specific for stabilizing boutons, as the other bouton subgroups were not affected.
464 Indeed, we found that LatB specifically increased the absolute density of stabilizing boutons
465 by almost 2-fold (Fig. 6D) and increased the fraction of axons with stabilizing boutons (Fig.
466 6E). The rapid and highly specific action of LatB suggests a direct action on the local actin
467 cytoskeleton. The changes in bouton dynamics after LatB treatment were surprisingly similar
468 to Sema4D treatment (Fig. 2F and 2K). Our findings suggest that inhibitory bouton dynamics

469 are regulated by specific changes in the actin cytoskeleton and that conditions favoring actin
470 depolymerization promote bouton stabilization.

471 The similarity between stabilization of inhibitory boutons induced by treatment with LatB or
472 Semaphorin 4D suggests that both treatments may induce a similar effect on intracellular actin. As
473 we found that only a specific subset of inhibitory boutons were stabilized by Semaphorin 4D
474 treatment (Fig. 2C), we wondered if these were the same boutons that responded to LatB. To
475 test this, we treated slices with a combination of LatB and Fc or LatB and Semaphorin 4D. We found
476 that bouton stabilization by LatB occluded a further increase by co-application with Semaphorin 4D
477 (Fig. 6F and 6G), although it did increase the fraction of new boutons. These results suggest
478 that LatB and Semaphorin 4D treatment act to stabilize a specific, overlapping, subset of inhibitory
479 boutons.

480 We then wondered if treatment with the actin depolymerizing drug LatB would be sufficient
481 to induce inhibitory synapse formation, similarly to the Semaphorin 4D treatment. Interestingly, we
482 observed that although LatB induced changes in VGAT and gephyrin puncta after 2 h (Fig.
483 7A-F), these changes were not coordinated and did not result in an increase in the density of
484 inhibitory synapses (Fig. 7G). Gephyrin and VGAT staining returned to baseline with longer
485 LatB treatment. Together, our data suggest that LatB and Semaphorin 4D induce rapid stabilization
486 of the same subgroup of inhibitory boutons, but that only Semaphorin 4D signaling leads to
487 coordinated pre- and postsynaptic changes resulting in inhibitory synapse formation. This
488 indicates that presynaptic bouton stabilization alone is not enough to induce inhibitory
489 synapse formation and that additional signaling may be required.

490

491 **Inhibitory bouton stabilization by Semaphorin 4D requires MET**

492 Our observation that LatB could mimic the Semaphorin 4D-induced stabilization of inhibitory
493 boutons points to a possible involvement of MET in this process. We therefore assessed if
494 MET activation is necessary for the observed Semaphorin 4D-induced stabilization of boutons by
495 making use of the highly specific MET inhibitor PHA-665752 (PHA) (Christensen et al.,
496 2003; Deguchi et al., 2016). We first verified that adding PHA alone did not affect bouton
497 dynamics (Fig. 8B) or spontaneous inhibitory postsynaptic currents (data not shown),
498 indicating that MET is not very active under baseline conditions in our slices. Next, we
499 treated our slices with Semaphorin 4D to induce bouton stabilization and compared bouton dynamics
500 in the presence or absence of PHA (Fig. 8A, C-D) Blocking MET with PHA completely
501 abolished the Semaphorin 4D-induced increase in the density of stabilizing boutons (Fig. 8D). In
502 fact, blocking MET in combination with Semaphorin 4D treatment almost entirely abolished the

503 occurrence of stabilizing boutons on our slices (Fig. 8E), while the other bouton subgroups
504 were not much affected (8C). Consistent with the live imaging data, inhibiting MET with
505 PHA also blocked the increase in VGAT staining intensity (Fig. 8F,G) and mIPSC frequency
506 (Fig. 8H) after Semaphorin 4D treatment. Taken together, these data indicate that activation of MET
507 is required for the Semaphorin 4D-induced stabilization of inhibitory boutons.

508 As the actin depolymerization pathway downstream of Semaphorin 4D/PlexinB1 signaling via MET
509 was previously shown to reduce intracellular RhoA activity (Swiercz et al., 2008; Sun et al.,
510 2012), we tested if stabilization of inhibitory boutons could also be achieved by directly
511 reducing ROCK activity, a well-known downstream effector of RhoA (Amano et al., 2010).
512 We found that reducing ROCK signaling with the specific ROCK inhibitor Y-27632 also
513 resulted in an increase in the density of stabilizing boutons in our slices (Fig. 8I), which was
514 similar to the effect of LatB and Semaphorin 4D treatments. This suggests that the intracellular
515 pathway that is activated by Semaphorin 4D/PlexinB1 signaling to induce stabilization of inhibitory
516 boutons involves activation of MET receptor tyrosine kinase and reduction of ROCK activity
517 to promote specific changes in the actin cytoskeleton.

518

519 **MET is enriched at a subset of inhibitory presynaptic boutons**

520 Our pharmacological experiments do not address if Semaphorin 4D-induced changes in actin occur
521 at the pre- or postsynaptic compartment. The subcellular localization of Semaphorin 4D and
522 PlexinB1 is not known (Paradis et al., 2007), but the localization of MET has been described.
523 Interestingly, it was reported that in postnatal tissue the majority of MET is localized in axons
524 (Judson et al., 2009) and detailed EM analysis showed clusters of MET in the shaft of
525 unmyelinated axons and in small presynaptic terminals (Eagleson et al., 2013). The majority
526 of these terminals are glutamatergic (Tyndall and Walikonis, 2006; Xie et al., 2016), but
527 possible MET expression in GABAergic axons was never addressed directly. To address the
528 localization of MET in our slices, we made use of an antibody (Qiu et al., 2014) and a
529 nanobody (Heukers et al., 2014) with demonstrated specificity for MET. We first confirmed
530 that both label synapses in primary hippocampal cultures (Fig. 9A-C). The majority of MET
531 puncta overlapped with excitatory synapses (Fig. 9A,B) in line with previous reports (Tyndall
532 and Walikonis, 2006; Eagleson et al., 2013; Xie et al., 2016). However, clear association of
533 MET with inhibitory presynapses was also observed in these cultures (Fig. 9B,C). We then
534 used the MET nanobody and antibody to label MET in our hippocampal slices of GAD65-
535 GFP mice (Fig. 9D). Although there was a quantitative difference, presumably reflecting a
536 difference in labeling affinity, both methods clearly showed that a subset of GFP-labeled

537 inhibitory boutons was enriched for MET (Fig. 9E). Comparison between the MET staining
538 pattern with staining for postsynaptic gephyrin (compare Figs. 9F and 3F) suggests a
539 presynaptic localization of MET at these inhibitory synapses, as MET puncta were often
540 completely embedded in the GFP-labeled bouton. These data suggest that MET may be
541 present in inhibitory axons and terminals to mediate Sema4D/plexinB1 signaling.
542

543 **DISCUSSION**

544

545 By monitoring individual boutons over time in live brain slices, we observed that the primary
546 action of Sema4D signaling is to stabilize presynaptic boutons of inhibitory axons within tens
547 of minutes. These stabilizing boutons develop into mature, functional inhibitory synapses over
548 the course of several hours. They rapidly acquire presynaptic vesicles as evidenced by an
549 increase in VGAT staining, while recruitment of postsynaptic gephyrin was slower. We
550 demonstrate for the first time that Sema4D-induced bouton stabilization is activity-dependent
551 and that Sema4D signaling can induce local changes in bouton density. We found that
552 inhibitory axons respond differently to Sema4D signaling in active and inactive networks
553 (Fig. 5). These results suggest that inhibitory axons can respond very rapidly to local signals
554 in their environment, but that the response is modulated by the state of the network and/or the
555 local internal state of the axon. It was previously shown that Sema4D in inhibitory synapses
556 signals via the PlexinB1 receptor. We now show that this signaling pathway requires co-
557 activation of the receptor tyrosine kinase MET. The downstream intracellular pathway
558 involves specific remodeling of the actin cytoskeleton, which can be mimicked by bath
559 application of low levels of the actin depolymerizing drug LatB or by reducing ROCK
560 activity. Our immunohistochemistry data suggest that MET is localized to the presynaptic
561 compartment of GABAergic synapses. Our data is the first to show a role for the autism-
562 linked MET in inhibitory synapses.

563

564 Our live imaging experiments give unique insight in the dynamics of inhibitory synapse
565 formation in brain slices, which remain undetected with methods using stationary
566 comparisons before and after treatment. In our slices, the majority of GFP-labeled boutons are
567 persistent and display pre- and postsynaptic markers of mature inhibitory synapses, but a
568 significant portion (~20-25%) of inhibitory boutons are non-persistent and represent locations
569 where inhibitory synapses are ‘in transition’. At these axonal locations, inhibitory synapses
570 are formed and disassembled in an apparent trial-and-error fashion (Wierenga et al., 2008;
571 Dobie and Craig, 2011; Fu et al., 2012; Schuemann et al., 2013; Wierenga, 2017). We found
572 that Sema4D signaling did not induce formation of inhibitory synapses *de novo*, but
573 specifically stabilized boutons at locations where a bouton had occurred before. We also
574 observed that Sema4D-induced bouton stabilization was not further enhanced by longer
575 treatment (>2 h) or by co-application with LatB, suggesting that the number of boutons

576 susceptible to Semaphorin 4D at any given time is limited. This suggests that Semaphorin 4D signaling is
577 involved only at a specific stage during synapse formation and that boutons which are more
578 mature or too immature do not respond to Semaphorin 4D. In primary cultures, a larger fraction of
579 synapses are immature compared to intact tissue (Dobie and Craig, 2011; Kuriu et al., 2012),
580 which may explain why the Semaphorin 4D effect on inhibitory synapses is stronger in primary
581 neurons (Kuzirian et al., 2013). In our slices, Semaphorin 4D treatment increased inhibitory synapse
582 density by ~20% after 24 hours (Fig. 3G), which is comparable to experience-dependent
583 changes in inhibitory synapses observed *in vivo* (Keck et al., 2011; Chen et al., 2015; Villa et
584 al., 2016).

585
586 One of the key observations of this study is that the primary action of Semaphorin 4D is to stabilize
587 presynaptic boutons of inhibitory axons within tens of minutes. These stabilizing boutons
588 develop into mature, functional inhibitory synapses over the course of several hours. It was
589 previously shown that inhibitory synapses can be induced by postsynaptic gephyrin clustering
590 (Flores et al., 2015), and rapid formation of new gephyrin clusters was observed after
591 Semaphorin 4D treatment in primary cultures (Kuzirian et al., 2013), suggesting that Semaphorin 4D may
592 promote inhibitory synapse formation via a postsynaptic mechanism. However, our data
593 clearly show that gephyrin clustering after Semaphorin 4D treatment is delayed and that the primary
594 action of Semaphorin 4D signaling is presynaptic bouton stabilization, arguing against a triggering
595 mechanism via postsynaptic gephyrin. The increase in VGAT signal reflects recruitment of
596 synaptic vesicles to newly forming synapses (Dobie and Craig, 2011; Schuemann et al.,
597 2013). Bouton stabilization and gephyrin clustering were also induced by LatB, but LatB
598 failed to induce new inhibitory synapses. This suggests that Semaphorin 4D signaling coordinates
599 pre- and postsynaptic changes at emerging inhibitory synapses. The faster time course for the
600 increase in postsynaptic gephyrin clusters in primary cultures (Kuzirian et al., 2013) may
601 reflect an overall difference in neuronal maturation level. In young neurons, new gephyrin
602 clusters can be rapidly induced by local GABA signaling (Oh et al., 2016), while in mature
603 neurons prolonged or additional signaling may be required.

604
605 It was previously shown that Semaphorin 4D acts as a postsynaptic protein and requires PlexinB1 for
606 promoting inhibitory synapse formation (Kuzirian et al., 2013; Raissi et al., 2013). Our data
607 shows that this signaling pathway requires co-activation of MET, suggesting that the receptor
608 tyrosine kinase MET acts as a co-receptor of PlexinB1 (Swiercz et al., 2008). PlexinB1 and
609 MET receptors can form a complex which, upon Semaphorin 4D stimulation, results in cross-

610 activation of both receptors (Giordano et al., 2002). It is currently not known if the PlexinB1
611 receptors that mediate the Sema4D signaling are located in the pre-or postsynaptic membrane
612 and our data does not address this issue directly. However, our immunohistochemistry data
613 (Fig. 9) suggest that MET receptors are localized in a subset of inhibitory synapses, in
614 primary hippocampal cultures and organotypic slices. A presynaptic location of MET in
615 inhibitory boutons suggests retrograde signaling of postsynaptic Sema4D via presynaptic
616 plexinB1 receptors. Retrograde semaphorin signaling was recently demonstrated in
617 *Drosophila* neuromuscular junction (Orr et al., 2017). However, cell-specific genetic studies
618 will be needed to rule out a contribution of Sema4D signaling via postsynaptic receptors in
619 inhibitory synapse formation.

620

621 Our data indicates that inhibitory bouton stabilization by activation of the Sema4D/PlexinB1
622 signaling pathway is induced through actin remodeling (Swiercz et al., 2008; Sun et al.,
623 2012). The induced changes in actin are highly specific and not due to a general decrease in
624 actin dynamics since Jasplakinolide did not affect inhibitory boutons. Treatment with the actin
625 depolymerizing drug LatB or the ROCK inhibitor Y-27632 promoted bouton stabilization in a
626 similar way as Sema4D, presumably by inducing similar changes in presynaptic actin at
627 stabilizing boutons. Given that actin is abundantly present in all cells, it is surprising that bath
628 application of LatB specifically promotes stabilization of immature boutons without affecting
629 other inhibitory boutons. It is important to note that low doses of monomer sequestering
630 drugs, such as LatB, do not lead to the complete disassembly of actin structures and leave
631 postsynaptic spines and synaptic transmission intact (Honkura et al., 2008; Rex et al., 2009;
632 Bleckert et al., 2012). Instead, LatB treatment may result in limited availability of actin
633 monomers in small cellular compartments, which indirectly affects actin-regulating factors
634 resulting in structural changes of the actin cytoskeleton (Ganguly et al., 2015; Suarez et al.,
635 2015). Our data therefore suggest that the actin cytoskeleton at stabilizing boutons is different
636 from other compartments and specifically sensitive to LatB. However, we stress here that our
637 experiments cannot distinguish between pre- or postsynaptic effects of LatB, but the rapid
638 (boutons are stabilized within 10 minutes) and highly specific effect seems to suggest a local
639 action of LatB. Inhibitory synapses are usually localized directly on the dendritic shaft and not
640 much is known about a possible role of postsynaptic actin structures at these synapses. Within
641 axons, several actin-based structures have been described (Leterrier et al., 2017) and
642 presynaptic actin has been implicated in transmission, plasticity, as well as synapse formation
643 (Cingolani and Goda, 2008; Chia et al., 2013). In *C. elegans* and *Drosophila* it has been

644 demonstrated that presynaptic actin structures undergo important remodeling during synapse
645 formation (Chia et al., 2014; Piccioli and Littleton, 2014). It is currently not known which
646 actin-regulating factors are involved in presynaptic bouton stabilization, but promising
647 candidates include cortactin (Alicea et al., 2017), cofilin (Piccioli and Littleton, 2014) and
648 Mical (Orr et al., 2017). Future studies will be necessary to unravel precise actin structures in
649 mature and immature boutons and the role of actin-regulating factors during synapse
650 formation.

651

652 Changes in inhibitory synapses play an important role in the rewiring of circuits during
653 development and in response to behavioral demands during adulthood (Keck et al., 2011;
654 Chen et al., 2015; Froemke, 2015) and defects in GABAergic synapses are associated with
655 neurodevelopmental diseases (Hensch, 2004; Marín, 2012). Mutations in the MET gene are an
656 established risk factor for autism spectrum disorder (ASD), as determined by various human
657 imaging and genetic studies (Peng et al., 2013). It is a multifunctional receptor involved in
658 many cellular pathways, and its exact role in ASD is not yet understood (Eagleson et al.,
659 2017). Previous studies in neurons have implicated MET in regulating postsynaptic strength
660 in excitatory neurons (Qiu et al., 2014; Lo et al., 2016), excitatory synapse formation (Xie et
661 al., 2016) and interneuron migration (Martins et al., 2011). Our data demonstrate that
662 activation of MET is also an essential part of the Sema4D-signaling pathway promoting
663 activity-dependent inhibitory bouton stabilization, indicating a novel role of MET in the
664 assembly of inhibitory presynapses.

665

666

667 REFERENCES

- 668 Alicea D, Perez M, Maldonado C, Dominicci-Cotto C, Marie X (2017) Cortactin Is a Regulator of Activity-
669 Dependent Synaptic Plasticity Controlled by Wingless. *J Neurosci* 37:2203–2215 Available at:
670 <http://www.jneurosci.org/content/jneuro/37/8/2203.full.pdf>.
- 671 Amano M, Nakayama M, Kaibuchi K (2010) Rho-kinase/ROCK: A key regulator of the cytoskeleton and cell
672 polarity. *Cytoskeleton* 67:545–554 Available at: <http://www.ncbi.nlm.nih.gov/pubmed/20803696>
673 [Accessed December 4, 2017].
- 674 Basile JR, Holmbeck K, Bugge TH, Gutkind JS (2007) MT1-MMP controls tumor-induced angiogenesis through
675 the release of semaphorin 4D. *J Biol Chem* 282:6899–6905 Available at:
676 <http://www.ncbi.nlm.nih.gov/pubmed/17204469> [Accessed August 29, 2013].
- 677 Bleckert A, Photowala H, Alford S (2012) Dual pools of actin at presynaptic terminals. *J Neurophysiol*
678 107:3479–3492 Available at: <http://jn.physiology.org/cgi/doi/10.1152/jn.00789.2011> [Accessed October
679 10, 2014].
- 680 Bury LA, Sabo SL (2016) Building a Terminal: Mechanisms of Presynaptic Development in the CNS. *Neurosci*
681 22:372–391 Available at: <http://www.ncbi.nlm.nih.gov/pubmed/26208860>.
- 682 Cagnoni G, Tamagnone L (2014) Semaphorin receptors meet receptor tyrosine kinases on the way of tumor
683 progression. *Oncogene* 33:4795–4802 Available at: <http://dx.doi.org/10.1038/onc.2013.474>.
- 684 Caroni P, Donato F, Muller D (2012) Structural plasticity upon learning: regulation and functions. *Nat Rev*
685 *Neurosci* 13:478–490 Available at: <http://dx.doi.org/10.1038/nrn3258>.
- 686 Cellot G, Cherubini E (2014) GABAergic signaling as therapeutic target for autism spectrum disorders. *Front*
687 *Pediatr* 2:70 Available at:
688 [http://www.pubmedcentral.nih.gov/articlerender.fcgi?artid=4085902&tool=pmcentrez&rendertype=abstra](http://www.pubmedcentral.nih.gov/articlerender.fcgi?artid=4085902&tool=pmcentrez&rendertype=abstract)
689 [ct](http://www.pubmedcentral.nih.gov/articlerender.fcgi?artid=4085902&tool=pmcentrez&rendertype=abstract).
- 690 Chen SX, Kim AN, Peters AJ, Komiyama T (2015) Subtype-specific plasticity of inhibitory circuits in motor
691 cortex during motor learning. *Nat Neurosci* 18:1109–1115 Available at:
692 [http://www.nature.com/neuro/journal/v18/n8/full/nn.4049.html?WT.ec_id=NEURO-](http://www.nature.com/neuro/journal/v18/n8/full/nn.4049.html?WT.ec_id=NEURO-201508&spMailingID=49196618&spUserID=MTMyMDY4MzI3NDgzS0&spJobID=723694367&spRepo)
693 [201508&spMailingID=49196618&spUserID=MTMyMDY4MzI3NDgzS0&spJobID=723694367&spRepo](http://www.nature.com/neuro/journal/v18/n8/full/nn.4049.html?WT.ec_id=NEURO-201508&spMailingID=49196618&spUserID=MTMyMDY4MzI3NDgzS0&spJobID=723694367&spRepo)
694 [rtId=NzIzNjk0MzY3S0%5Cnhttp://www.nature.com/neuro/journal/v18/n8/pdf/nn.4049.pdf](http://www.nature.com/neuro/journal/v18/n8/pdf/nn.4049.pdf).
- 695 Chia PH, Chen B, Li P, Rosen MK, Shen K (2014) Local F-actin network links synapse formation and axon
696 branching. *Cell* 156:208–220 Available at: <http://dx.doi.org/10.1016/j.cell.2013.12.009> [Accessed January
697 21, 2014].
- 698 Chia PH, Li P, Shen K (2013) Cellular and molecular mechanisms underlying presynapse formation. *J Cell Biol*
699 203:11–22 Available at: <http://www.ncbi.nlm.nih.gov/pubmed/24127213> [Accessed January 28, 2014].
- 700 Christensen JG, Schreck R, Burrows J, Kuruganti P, Chan E, Le P, Chen J, Wang X, Ruslim L, Blake R, Lipson
701 KE, Ramphal J, Do S, Cui JJ, Cherrington JM, Mendel DB (2003) A Selective Small Molecule Inhibitor of
702 c-Met Kinase Inhibits c-Met-Dependent Phenotypes in Vitro and Exhibits Cytoreductive Antitumor
703 Activity in Vivo. *Cancer Res* 63:7345–7355.
- 704 Cingolani LA, Goda Y (2008) Actin in action: the interplay between the actin cytoskeleton and synaptic
705 efficacy. *Nat Rev Neurosci* 9:344–356 Available at: <http://www.nature.com/doi/doi/10.1038/nrn2373>.
- 706 Deguchi Y, Harada M, Shinohara R, Lazarus M, Cherasse Y, Urade Y, Yamada D, Sekiguchi M, Watanabe D,
707 Furuyashiki T, Narumiya S (2016) mDia and ROCK Mediate Actin-Dependent Presynaptic Remodeling
708 Regulating Synaptic Efficacy and Anxiety. *Cell Rep* 17:2405–2417 Available at:
709 <http://dx.doi.org/10.1016/j.celrep.2016.10.088>.
- 710 Dobie FA, Craig AM (2011) Inhibitory Synapse Dynamics: Coordinated Presynaptic and Postsynaptic Mobility
711 and the Major Contribution of Recycled Vesicles to New Synapse Formation. *J Neurosci* 31:10481–10493
712 Available at: <http://www.jneurosci.org/cgi/doi/10.1523/JNEUROSCI.6023-10.2011> [Accessed July 20,
713 2011].

- 714 Eagleson KL, Milner TA, Xie Z, Levitt P (2013) Synaptic and extrasynaptic location of the receptor tyrosine
715 kinase met during postnatal development in the mouse neocortex and hippocampus. *J Comp Neurol*
716 521:3241–3259 Available at:
717 <http://www.pubmedcentral.nih.gov/articlerender.fcgi?artid=3942873&tool=pmcentrez&rendertype=abstract>
718 [Accessed November 21, 2014].
- 719 Eagleson KL, Xie Z, Levitt P (2017) The Pleiotropic MET Receptor Network: Circuit Development and the
720 Neural-Medical Interface of Autism. *Biol Psychiatry* 81:424–433 Available at:
721 <http://linkinghub.elsevier.com/retrieve/pii/S0006322316327780>.
- 722 Esteves da Silva M, Adrian M, Schätzle P, Lipka J, Watanabe T, Cho S, Futai K, Wierenga CJ, Kapitein LC,
723 Hoogenraad CC, Schätzle P, Lipka J, Watanabe T, Cho S, Futai K, Wierenga CJ, Kapitein LC,
724 Hoogenraad CC (2015) Positioning of AMPA Receptor-Containing Endosomes Regulates Synapse
725 Architecture. *Cell Rep* 13:933–943 Available at: <http://www.ncbi.nlm.nih.gov/pubmed/26565907>
726 [Accessed November 16, 2015].
- 727 Flores CE, Nikonenko I, Mendez P, Fritschy J-M, Tyagarajan SK, Muller D (2015) Activity-dependent
728 inhibitory synapse remodeling through gephyrin phosphorylation. *Proc Natl Acad Sci* 112:E65–E72
729 Available at: <http://www.pnas.org/lookup/doi/10.1073/pnas.1411170112>.
- 730 Frias CP, Wierenga CJ (2013) Activity-dependent adaptations in inhibitory axons. *Front Cell Neurosci* 7:219
731 Available at: <http://www.ncbi.nlm.nih.gov/pubmed/24312009> [Accessed December 12, 2013].
- 732 Froemke RC (2015) Plasticity of Cortical Excitatory-Inhibitory Balance. *Annu Rev Neurosci* 38:195–219
733 Available at: <http://www.ncbi.nlm.nih.gov/pubmed/25897875> [Accessed April 30, 2015].
- 734 Fu Y, Huang ZJ (2010) Differential dynamics and activity-dependent regulation of α - and β -neurexins at
735 developing GABAergic synapses. *Proc Natl Acad Sci U S A* 107:22699–22704 Available at:
736 <http://www.ncbi.nlm.nih.gov/pubmed/21149722> [Accessed January 3, 2011].
- 737 Fu Y, Wu X, Lu J, Huang ZJ (2012) Presynaptic GABAB Receptor Regulates Activity-Dependent Maturation
738 and Patterning of Inhibitory Synapses through Dynamic Allocation of Synaptic Vesicles. *Front Cell*
739 *Neurosci* 6:1–20 Available at:
740 http://www.frontiersin.org/Cellular_Neuroscience/10.3389/fncel.2012.00057/abstract [Accessed December
741 10, 2012].
- 742 Ganguly A, Tang Y, Wang L, Ladt K, Loi J, Dargent B, Leterrier C, Roy S (2015) A dynamic formin-dependent
743 deep F-actin network in axons. *J Cell Biol* 210:401–417 Available at:
744 <http://www.jcb.org/cgi/doi/10.1083/jcb.201506110>.
- 745 Giacobini P, Messina A, Morello F, Ferraris N, Corso S, Penachioni J, Giordano S, Tamagnone L, Fasolo A
746 (2008) Semaphorin 4D regulates gonadotropin hormone-releasing hormone-1 neuronal migration through
747 PlexinB1-Met complex. *J Cell Biol* 183:555–566.
- 748 Giordano S, Corso S, Conrotto P, Artigiani S, Gilestro G, Barberis D, Tamagnone L, Comoglio PM (2002) The
749 semaphorin 4D receptor controls invasive growth by coupling with Met. *Nat Cell Biol* 4:720–724
750 Available at: <http://www.ncbi.nlm.nih.gov/pubmed/12198496> [Accessed April 11, 2016].
- 751 Hensch TK (2004) Critical Period Regulation. *Annu Rev Neurosci* 27:549–579 Available at:
752 <http://www.annualreviews.org/doi/10.1146/annurev.neuro.27.070203.144327>.
- 753 Hensch TK (2005) Critical period plasticity in local cortical circuits. *Nat Rev Neurosci* 6:877–888 Available at:
754 <http://www.ncbi.nlm.nih.gov/pubmed/16261181>.
- 755 Heukers R, Altintas I, Raghoenath S, De Zan E, Pepermans R, Roovers RC, Haselberg R, Hennink WE,
756 Schiffelers RM, Kok RJ, Van Bergen en Henegouwen PMP (2014) Targeting hepatocyte growth factor
757 receptor (Met) positive tumor cells using internalizing nanobody-decorated albumin nanoparticles.
758 *Biomaterials* 35:601–610 Available at: <http://dx.doi.org/10.1016/j.biomaterials.2013.10.001>.
- 759 Honkura N, Matsuzaki M, Noguchi J, Ellis-Davies GCR, Kasai H (2008) The subsynaptic organization of actin
760 fibers regulates the structure and plasticity of dendritic spines. *Neuron* 57:719–729 Available at:
761 <http://www.ncbi.nlm.nih.gov/pubmed/18341992> [Accessed July 4, 2011].

- 762 Isaacson JS, Scanziani M (2011) How inhibition shapes cortical activity. *Neuron* 72:231–243 Available at:
763 <http://www.ncbi.nlm.nih.gov/pubmed/22017986> [Accessed July 14, 2012].
- 764 Judson MC, Bergman MY, Campbell DB, Eagleson KL, Levitt P (2009) Dynamic gene and protein expression
765 patterns of the autism-associated met receptor tyrosine kinase in the developing mouse forebrain. *J Comp*
766 *Neurol* 513:511–531.
- 767 Keck T, Scheuss V, Jacobsen RI, Wierenga CJ, Eysel UT, Bonhoeffer T, Hübener M (2011) Loss of sensory
768 input causes rapid structural changes of inhibitory neurons in adult mouse visual cortex. *Neuron* 71:869–
769 882 Available at: <http://linkinghub.elsevier.com/retrieve/pii/S0896627311005642> [Accessed September 9,
770 2011].
- 771 Kolodkin AL, Matthes DJ, Goodman CS (1993) The semaphorin genes encode a family of transmembrane and
772 secreted growth cone guidance molecules. *Cell* 75:1389–1399.
- 773 Krueger-Burg D, Papadopoulos T, Brose N (2017) Organizers of inhibitory synapses come of age. *Curr Opin*
774 *Neurobiol* 45:66–77 Available at: <http://dx.doi.org/10.1016/j.conb.2017.04.003>.
- 775 Kuriu T, Yanagawa Y, Konishi S (2012) Activity-dependent coordinated mobility of hippocampal inhibitory
776 synapses visualized with presynaptic and postsynaptic tagged-molecular markers. *Mol Cell Neurosci*
777 49:184–195 Available at: <http://www.ncbi.nlm.nih.gov/pubmed/22146684> [Accessed December 12, 2011].
- 778 Kuzirian MS, Moore AR, Staudenmaier EK, Friedel RH, Paradis S (2013) The class 4 semaphorin Sema4D
779 promotes the rapid assembly of GABAergic synapses in rodent hippocampus. *J Neurosci* 33:8961–8973
780 Available at: <http://www.ncbi.nlm.nih.gov/pubmed/23699507> [Accessed May 22, 2013].
- 781 Leterrier C, Dubey P, Roy S (2017) The nano-architecture of the axonal cytoskeleton. *Nat Rev Neurosci* 18:713–
782 726 Available at: <http://www.nature.com/doi/10.1038/nrn.2017.129>.
- 783 Lo F-S, Erzurumlu RS, Powell EM (2016) Insulin-Independent GABAA Receptor-Mediated Response in the
784 Barrel Cortex of Mice with Impaired Met Activity. *J Neurosci* 36:3691–3697 Available at:
785 <http://www.ncbi.nlm.nih.gov/pubmed/27030755> [Accessed May 18, 2016].
- 786 López-Bendito G, Sturgess K, Erdélyi F, Szabó G, Molnár Z, Paulsen O (2004) Preferential origin and layer
787 destination of GAD65-GFP cortical interneurons. *Cereb Cortex* 14:1122–1133 Available at:
788 <http://www.ncbi.nlm.nih.gov/pubmed/15115742>.
- 789 Lu W, Bromley-Coolidge S, Li J (2017) Regulation of GABAergic synapse development by postsynaptic
790 membrane proteins. *Brain Res Bull* 129:30–42.
- 791 Marín O (2012) Interneuron dysfunction in psychiatric disorders. *Nat Rev Neurosci* 13:107–120 Available at:
792 <http://www.ncbi.nlm.nih.gov/pubmed/22251963> [Accessed October 9, 2012].
- 793 Martins GJ, Shahrokh M, Powell EM (2011) Genetic disruption of Met signaling impairs GABAergic striatal
794 development and cognition. *Neuroscience* 176:199–209 Available at:
795 <http://dx.doi.org/10.1016/j.neuroscience.2010.12.058> [Accessed May 18, 2016].
- 796 Müllner FE, Wierenga CJ, Bonhoeffer T (2015) Precision of inhibition: dendritic inhibition by individual
797 GABAergic synapses on hippocampal pyramidal cells is confined in space and time. *Neuron* 87:576–589.
- 798 Nelson SB, Valakh V (2015) Excitatory/Inhibitory Balance and Circuit Homeostasis in Autism Spectrum
799 Disorders. *Neuron* 87:684–698 Available at:
800 <http://linkinghub.elsevier.com/retrieve/pii/S0896627315006753>.
- 801 Oh WC, Lutz S, Castillo PE, Kwon H (2016) De novo synaptogenesis induced by GABA in the developing
802 mouse cortex. *Science* (80-) 5206.
- 803 Oinuma I, Katoh H, Negishi M (2006) Semaphorin 4D/Plexin-B1-mediated R-Ras GAP activity inhibits cell
804 migration by regulating $\beta 1$ integrin activity. *J Cell Biol* 173:601–613.
- 805 Orr BO, Fetter RD, Davis GW (2017) Retrograde semaphorin–plexin signalling drives homeostatic synaptic
806 plasticity. *Nature* 550:109–113 Available at: <http://www.nature.com/doi/10.1038/nature24017>.

- 807 Paradis S, Harrar DB, Lin Y, Koon AC, Hauser JL, Griffith EC, Zhu L, Brass LF, Chen C, Greenberg ME
808 (2007) An RNAi-based approach identifies molecules required for glutamatergic and GABAergic synapse
809 development. *Neuron* 53:217–232 Available at:
810 <http://linkinghub.elsevier.com/retrieve/pii/S0896627306009974>.
- 811 Pasterkamp RJ (2012) Getting neural circuits into shape with semaphorins. *Nat Rev Neurosci* 13:605–618
812 Available at: <http://dx.doi.org/10.1038/nrn3302>.
- 813 Peng Y, Huentelman M, Smith C, Qiu S (2013) MET Receptor Tyrosine Kinase as an Autism Genetic Risk
814 Factor. *Int Rev Neurobiol* 113:135–165.
- 815 Piccioli ZD, Littleton JT (2014) Retrograde BMP signaling modulates rapid activity-dependent synaptic growth
816 via presynaptic LIM kinase regulation of cofilin. *J Neurosci* 34:4371–4381 Available at:
817 <http://www.ncbi.nlm.nih.gov/pubmed/24647957>.
- 818 Qiu S, Lu Z, Levitt P (2014) MET Receptor Tyrosine Kinase Controls Dendritic Complexity, Spine
819 Morphogenesis, and Glutamatergic Synapse Maturation in the Hippocampus. *J Neurosci* 34:16166–16179
820 Available at: <http://www.jneurosci.org/cgi/doi/10.1523/JNEUROSCI.2580-14.2014>.
- 821 Raissi AJ, Staudenmaier EK, David S, Hu L, Paradis S (2013) Sema4D localizes to synapses and regulates
822 GABAergic synapse development as a membrane-bound molecule in the mammalian hippocampus. *Mol*
823 *Cell Neurosci* 57:23–32 Available at: <http://www.ncbi.nlm.nih.gov/pubmed/24036351> [Accessed
824 September 20, 2013].
- 825 Rex CS, Chen LY, Sharma A, Liu J, Babayan AH, Gall CM, Lynch G (2009) Different Rho GTPase-dependent
826 signaling pathways initiate sequential steps in the consolidation of long-term potentiation. *J Cell Biol*
827 186:85–97.
- 828 Schuemann A, Klawiter A, Bonhoeffer T, Wierenga CJ (2013) Structural plasticity of GABAergic axons is
829 regulated by network activity and GABAA receptor activation. *Front Neural Circuits* 7:1–16 Available at:
830 <http://journal.frontiersin.org/article/10.3389/fncir.2013.00113/abstract>.
- 831 Siddiqui TJ, Craig AM (2011) Synaptic organizing complexes. *Curr Opin Neurobiol* 21:132–143 Available at:
832 <http://www.pubmedcentral.nih.gov/articlerender.fcgi?artid=3016466&tool=pmcentrez&rendertype=abstract>
833 [Accessed August 15, 2013].
- 834 Sprekeler H (2017) Functional consequences of inhibitory plasticity: homeostasis, the excitation-inhibition
835 balance and beyond. *Curr Opin Neurobiol* 43:198–203 Available at:
836 <http://dx.doi.org/10.1016/j.conb.2017.03.014>.
- 837 Staras K (2007) Share and share alike: trading of presynaptic elements between central synapses. *Trends*
838 *Neurosci* 30:292–298 Available at: <http://www.ncbi.nlm.nih.gov/pubmed/17467066>.
- 839 Suarez C, Carroll RT, Burke TA, Christensen JR, Bestul AJ, Sees JA, James ML, Sirotkin V, Kovar DR (2015)
840 Profilin regulates F-Actin network homeostasis by favoring formin over Arp2/3 complex. *Dev Cell* 32:43–
841 53.
- 842 Sun T, Krishnan R, Swiercz JM (2012) Grb2 mediates semaphorin-4D-dependent RhoA inactivation. *J Cell Sci*
843 125:3557–3567 Available at: <http://www.ncbi.nlm.nih.gov/pubmed/22505611> [Accessed August 19,
844 2013].
- 845 Swiercz JM, Worzfeld T, Offermanns S (2008) ErbB-2 and Met reciprocally regulate cellular signaling via
846 plexin-B1. *J Biol Chem* 283:1893–1901 Available at: <http://www.ncbi.nlm.nih.gov/pubmed/18025083>
847 [Accessed August 19, 2013].
- 848 Tyndall SJ, Walikonis RS (2006) The receptor tyrosine kinase met and its ligand hepatocyte growth factor are
849 clustered at excitatory synapses and can enhance clustering of synaptic proteins. *Cell Cycle* 5:1560–1568.
- 850 Villa KL, Berry KP, Subramanian J, Cha JW, Oh WC, Kwon H-B, Kubota Y, So PTC, Nedivi E (2016)
851 Inhibitory Synapses Are Repeatedly Assembled and Removed at Persistent Sites In Vivo. *Neuron* 89:756–
852 769 Available at: <http://linkinghub.elsevier.com/retrieve/pii/S0896627316000118>.

- 853 Wierenga CJ (2017) Live imaging of inhibitory axons: Synapse formation as a dynamic trial-and-error process.
854 *Brain Res Bull* 129:43–49 Available at: <http://dx.doi.org/10.1016/j.brainresbull.2016.09.018>.
- 855 Wierenga CJ, Becker N, Bonhoeffer T (2008) GABAergic synapses are formed without the involvement of
856 dendritic protrusions. *Nat Neurosci* 11:1044–1052 Available at:
857 <http://www.ncbi.nlm.nih.gov/pubmed/18711391>.
- 858 Wierenga CJ, Müllner FE, Rinke I, Keck T, Stein V, Bonhoeffer T (2010) Molecular and electrophysiological
859 characterization of GFP-expressing CA1 interneurons in GAD65-GFP mice. *PLoS One* 5:e15915
860 Available at:
861 <http://www.pubmedcentral.nih.gov/articlerender.fcgi?artid=3013138&tool=pmcentrez&rendertype=abstract>
862 [Accessed March 10, 2012].
- 863 Xie Z, Eagleson KL, Wu H-H, Levitt P (2016) Hepatocyte Growth Factor Modulates MET Receptor Tyrosine
864 Kinase and β -Catenin Functional Interactions to Enhance Synapse Formation. *Eneuro* 3:e0074.
- 865 Zhou Y, Gunput RAF, Pasterkamp RJ (2008) Semaphorin signaling: progress made and promises ahead. *Trends*
866 *Biochem Sci* 33:161–170.
- 867
- 868

869 **FIGURE LEGENDS**

870

871 **Figure 1. Classification of presynaptic inhibitory boutons by their dynamics.**

872 **(A)** Time-lapse two-photon images of two inhibitory boutons (blue arrowheads) along a
873 GAD65-GFP-labeled axon in the CA1 region of the hippocampus. These boutons were
874 present at all time points, and therefore categorized as persistent boutons. Only every second
875 image is shown for clarity. On the right, the same region is shown after fixation and staining
876 against vesicular GABA transporter (VGAT, magenta). The zoom shows a single optical
877 plane through the bouton to demonstrate overlap (white) of VGAT and GFP boutons. Time in
878 minutes. Scale bars 2 μm and 1 μm (zoom).

879 **(B1-5)** Same as in A, showing examples of new (B1; absent during baseline), lost (B2; absent
880 during wash-in), stabilizing (B3; non-persistent during baseline, and persistent during wash-
881 in), destabilizing (B4; persistent during baseline, and non-persistent during wash-in) and
882 transient (B5; non-persistent during both baseline and wash-in) boutons. Filled yellow
883 arrowheads indicate that the bouton is present, and empty yellow arrowheads indicate that the
884 bouton is absent at the time point shown.

885 **(C)** Average fraction of persistent (P) and non-persistent (NP) boutons at any given time
886 point, and average fraction of the 5 subgroups of non-persistent boutons normalized to the
887 total number of non-persistent boutons (N – new; L – lost; S – stabilizing; D – destabilizing;
888 T – transient).

889 **(D)** Percentage of time points in which boutons were present during baseline (white) and
890 wash-in (gray) periods. #: value for D was significantly different from N and T for wash-in
891 (χ^2 ; D vs N, $p = 0.002$; D vs T, $p = 0.002$).

892 **(E)** Fraction of boutons positive for VGAT and gephyrin per axon. Two-way ANOVA
893 analysis showed a significant effect on bouton type ($p = 0.0098$). For gephyrin, P vs T, $p =$
894 0.001 (Sidak's multiple comparisons test).

895 **(F)** Fraction of boutons co-localizing with VGAT or gephyrin as a function of bouton
896 lifetime (total number of time points (#TPs) present during the imaging period). Lost boutons
897 ('L' in C,D) were not included. χ^2 : TP2-5, $p = 0.21$; TP6-8, $p = 0.02$; TP9-11, $p = 0.13$; TP12-
898 14, $p = 0.35$; TP15, $p = 0.008$.

899 Confocal images in A are maximum intensity projections of 5-8 z stacks, while two-photon
900 images are maximum intensity projections of 13-15 z stacks. Data are represented as mean \pm
901 SEM. Data in C and D from 90 axons from 24 independent experiments, data in E and F from

902 21 axons from 5 independent experiments for the VGAT staining (P: n=282 boutons; N:
903 n=13; S: n=6; D: n=17; T: n=45) and from 15 axons from 4 independent experiments for the
904 gephyrin staining (P: n=232 boutons; N: n=15; S: n=6; D: n=15; T: n=39). In F, n=14-28 per
905 TP, except for TP15.

906

907 **Figure 2. Sema4D treatment promotes inhibitory bouton stabilization.**

908 **(A)** Time-lapse two-photon images of GFP-labeled inhibitory axons in the CA1 region of
909 the hippocampus during baseline (5 time points) and wash-in (10 time points; grey box) of 1
910 nM Fc - control (C; upper panel) or 1 nM Sema4D-Fc (S4D; bottom panel). Only every
911 second image is shown for clarity. Persistent (blue) and non-persistent (yellow) boutons are
912 indicated by arrowheads. Filled arrowheads indicate that the bouton is present, and empty
913 arrowheads indicate that the bouton is absent at that time point. Images are maximum
914 intensity projections of 11-18 z stacks. Time in minutes. Scale bar 5 μ m.

915 **(B)** Cumulative distribution of the change in mean bouton density during the wash-in
916 period compared to baseline after wash-in of C or S4D (MW, $p = 0.83$).

917 **(C)** Average fraction of subgroups of non-persistent boutons in C- and S4D-treated axons:
918 N – new (MW, $p = 0.86$); L – lost (MW, $p = 0.93$); S – stabilizing (MW, $p = 0.003$); D –
919 destabilizing (MW, $p = 0.25$); T – transient (MW, $p = 0.89$).

920 **(D-H)** Density of new (D; MW, $p = 0.41$), lost (E; MW, $p = 0.61$), stabilizing (F; MW, $p =$
921 0.003), destabilizing (G; MW, $p = 0.84$) and transient (H; MW, $p = 0.34$) boutons in axons
922 treated with 1 nM Fc (C) and 1 nM Sema4D-Fc (S4D). Each dot represents an individual
923 axon.

924 **(I)** Stabilization of inhibitory boutons, as determined by the change (compared to
925 baseline) in density of boutons that were present at 5 consecutive time points during the
926 imaging period: 0'-40' (baseline), 50'-90' (wash-in) and 100'-140' (wash-in). Two-way
927 ANOVA analysis showed a significant effect of both treatment ($p = 0.04$) and time ($p = 0.03$).

928 **(J)** Density of boutons that stabilized in the last 5 time points (TPs) (MW, $p = 0.0008$).

929 **(K)** Frequency distribution of the stabilizing bouton density in C- and S4D-treated axons
930 (χ^2 , $p = 0.03$).

931 Data are represented as mean \pm SEM. Data from 20 control axons (N=6) and 22 S4D-treated
932 axons (N=5).

933

934 **Figure 3. Sema4D increases overall inhibitory synaptic density.**

935 **(A)** Fraction of non-persistent boutons after treatment with 1 nM Fc (control; C) or 1 nM
936 Semaphorin 4D-Fc (S4D) for 6 hours (400 minutes of total treatment). N – new (MW, $p = 0.91$) L –
937 lost (MW, $p = 0.13$); S – stabilizing (MW, $p = 0.0003$); D – destabilizing (MW, $p = 0.16$); T –
938 transient (MW, $p = 0.02$).

939 **(B)** Density of non-persistent boutons after treatment with 1 nM Fc (C) or 1 nM Semaphorin 4D-
940 Fc (S4D) for 6 hours. N: MW, $p = 0.74$; L: MW, $p = 0.29$; S: MW, $p = 0.03$; D: MW, $p =$
941 0.09 ; T: MW, $p = 0.11$.

942 **(C)** Density of stabilizing boutons after treatment with Fc or S4D for 50, 100 and 400
943 minutes. Two-way ANOVA analysis showed that S4D increased bouton density independent
944 of time ($p = 0.0002$). At 100', $p = 0.005$ (Sidak's multiple comparisons test).

945 **(D)** Same as B, but for transient boutons. Two-Way ANOVA analysis indicated a
946 significant interaction between treatment and time (§; $p = 0.03$).

947 **(E)** Representative images of CA1 dendritic area of GAD65-GFP hippocampal slices
948 treated with 1 nM Fc (C) or 1 nM Semaphorin 4D-Fc (S4D) for 24 h, and immunostained for VGAT
949 (green) and gephyrin (magenta). Images are average intensity projections of 5 z stacks. Scale
950 bar 2 μm .

951 **(F)** Example of an inhibitory synapse (white box in D), identified as the apposition of
952 VGAT (green) and gephyrin (magenta) puncta. The respective xz and yz projections show the
953 close apposition of the two markers. Images are maximum intensity projections of 6 z stacks.
954 Scale bar 1 μm .

955 **(G)** Density of inhibitory synapses in slices treated with Fc or S4D for 24 h (MW, $p =$
956 0.03).

957 **(H)** Representative whole-cell voltage-clamp recordings of miniature inhibitory
958 postsynaptic currents (mIPSCs) from CA1 pyramidal cells in organotypic hippocampal slices
959 treated for 24 h with 1 nM Fc/DMSO (C) or 1 nM S4D/DMSO (S4D).

960 **(I-J)** Mean mIPSC amplitude (H) and frequency (I) in CA1 cells after 24 h treatment with
961 Fc or S4D (H: MW, $p = 0.35$; I: MW, $p = 0.008$).

962 **(K)** Cumulative distribution of inter-event interval (IEI) of mIPSCs.

963 Data are represented as mean \pm SEM. Data in A,B from 15 control axons (N=4) and 17 S4D-
964 treated axons (N=4), data in G from 15 control images (N=3) and 15 S4D images (N=3), and
965 data in H-K from 14 control cells (N=5) and 14 S4D-treated cells (N=7).

966

967 **Figure 4. VGAT and gephyrin undergo different changes in response to Semaphorin 4D.**

968 (A) Normalized area of presynaptic vesicular GABA transporter (VGAT) puncta (after
969 treatment with 1 nM S4D for 2 h, 6 h and 24 h). Dotted line represents control (treatment with
970 1nM Fc for 2 h, 6 h and 24 h). Two-way ANOVA analysis showed that S4D treatment
971 increased VGAT area independent of time ($p = 0.005$).

972 (B) Normalized density of VGAT puncta, after treatment with 1 nM S4D for 2 h, 6 h and
973 24 h. Dotted line represents control (treatment with 1nM Fc for 2 h, 6 h and 24 h).

974 (C) Cumulative distributions of the normalized area of VGAT after treatment with 1 nM
975 S4D for 2, 6 and 24 h. Black line represents the normalized control values. $p = 0.81$, $p = 0.08$
976 and $p = 0.14$ (KS) for 2, 6 and 24 h, respectively.

977 (D-E) Same as in A-B, but for normalized area (D) and density (E) of postsynaptic gephyrin
978 puncta. Two-way ANOVA analysis showed a significant effect of time ($p = 0.04$) and an
979 interaction between treatment and time (§; $p = 0.04$) in E.

980 (F) Same as in C, but for normalized gephyrin density. $p = 0.99$, $p = 0.99$ and $p < 0.0001$
981 (KS) for 2, 6 and 24 h, respectively.

982 Data are represented as mean \pm SEM. Data from 15-20 control images (N=3-4) and 15-20
983 S4D images (N=3-4) per time point.

984

985 **Figure 5. Sema4D induces local stabilization of inhibitory boutons.**

986 (A) Density of stabilizing boutons in axons treated with 1
987 nM Fc (C) and 1 nM Sema4D-Fc (S4D), in the presence of 0.5 μ M TTX (MW, $p = 0.17$).

988 (B) Stabilization of inhibitory boutons upon treatment
989 with C or S4D in the presence of 0.5 μ M TTX, determined by the change (compared to
990 baseline) in density of boutons that were present at 5 consecutive time points during the
991 imaging period: 0'-40' (baseline), 50'-90' (wash-in) and 100'-140' (wash-in). Two-way
992 ANOVA analysis showed a significant effect of treatment ($p = 0.01$). At 100'-140', $p = 0.04$
993 (Sidak's multiple comparisons test).

994 (C) Fraction of axons with stabilizing boutons in axons
995 treated with C or S4D, in normal or activity-depleted slices with TTX (χ^2 (p-values are
996 Bonferroni-corrected): C vs S4D, $p = 0.01$; C vs C+TTX, $p = 0.58$; C+TTX vs S4D+TTX, $p =$
997 0.22; S4D vs S4D+TTX, $p < 0.0001$).

998 (D) Frequency distribution of the stabilizing bouton
999 density in C- and S4D-treated axons, in the presence of 0.5 μ M TTX (χ^2 , $p = 0.17$).

1000 **(E)** Representative image of the local treatment of GFP-
1001 labeled inhibitory axons in the CA1 region of the hippocampus. The pipette was filled with
1002 Alexa568 (red) to visualize the area of the puff (yellow circle). Scale bar 10 μ m.

1003 **(F)** Same as B, but for local treatment with 10 nM Fc
1004 (control, C) or 10 nM S4D. Red line marks the puffing. Two-way ANOVA analysis showed a
1005 significant effect of treatment ($p = 0.0002$) and an interaction between treatment and time ($\$$;
1006 $p = 0.02$). At 50'-70', $p = 0.003$ (Sidak's multiple comparisons test).

1007 **(G)** Cumulative distribution of the change in mean bouton
1008 density after local treatment with C or S4D compared to baseline (MW, $p = 0.045$).
1009 Data are represented as mean \pm SEM. Data in A-D from 19 control axons (N=5) and 20 S4D-
1010 treated axons (N=5), and in F-G from 15 control axons (N=6) and 17 S4D-treated axons
1011 (N=6).

1012

1013 **Figure 6. Inhibitory bouton dynamics are regulated by actin.**

1014 **(A)** Time-lapse two-photon images of GAD65-GFP-labeled axons in the CA1 region of
1015 the hippocampus during baseline (5 time points) and wash-in (10 time points; grey box) of
1016 DMSO - control (C; upper panel), 200 nM Jasplakinolide (Jasp; middle panel) or 100 nM
1017 LatrunculinB (LatB; bottom panel). Only every second image is shown for clarity. Persistent
1018 and non-persistent boutons are indicated as in Figure 2. Images are maximum intensity
1019 projections of 12-14 z stacks. Time in minutes. Scale bar 5 μ m.

1020 **(B)** Fraction of non-persistent (NP) boutons in C and Jasp-treated axons: N – new (MW, p
1021 = 0.37); L – lost (MW, $p = 0.18$); S – stabilizing (MW, $p = 0.49$); D – destabilizing (MW, $p =$
1022 0.95); T – transient (MW, $p = 0.93$).

1023 **(C)** Same as in B, but for C and LatB-treated axons (N: MW, $p = 0.99$; L: MW, $p = 0.66$;
1024 S: MW, $p = 0.01$; D: MW, $p = 0.6$; T: MW, $p = 0.29$).

1025 **(D)** Density of stabilizing boutons in control, Jasp- (MW: $p = 0.55$) and LatB-treated
1026 axons (MW: $p = 0.005$).

1027 **(E)** Frequency distribution of the stabilizing bouton density in C, Jasp- and LatB-treated
1028 slices (χ^2 ; C vs Jasp, $p = 0.31$; C vs LatB, $p = 0.0005$).

1029 **(F)** Same as E, but for combined treatment with 100 nM LatB/1 nM Fc (LatB+C) or 100
1030 nM LatB/1 nM Sema4D (LatB+S4D) (χ^2 , $p = 0.37$).

1031 **(G)** Same as B, but for combined treatment with LatB+C or LatB+S4D (N: MW, $p =$
1032 0.005; L: MW, $p = 0.58$; S: MW, $p = 0.96$; D: MW, $p = 0.82$; T: MW, $p = 0.52$).

1033 Data are represented as mean \pm SEM. Data in B from 21 control axons (N=6) and 20 Jasp-
1034 treated axons (N=5), in C from 18 control axons (N=5) and 20 LatB-treated axons (N=5) and
1035 in F-G from 18 LatB+Fc- (N=4) and 20 LatB+S4D-treated axons (N=5).

1036

1037 **Figure 7. Latrunculin B treatment does not promote inhibitory synapse formation.**

1038 (A) Normalized area of presynaptic vesicular GABA transporter (VGAT) puncta (after
1039 treatment with 100 nM LatB for 2 h and 24 h). Dotted line represents control (treatment with
1040 DMSO for 2 h and 24 h). Two-way ANOVA analysis indicated a significant effect of time (p
1041 = 0.02) and an interaction between treatment and time (§, $p = 0.02$).

1042 (B) Normalized density of VGAT, after treatment with 100 nM LatB for 2 h and 24 h.
1043 Dotted line represents control (treatment with DMSO for 2 h and 24 h).

1044 (C) Cumulative distributions of the normalized area of VGAT after treatment with 100 nM
1045 LatB for 2 and 24 h. Black line represents the normalized control values. $p = 0.047$ and 0.33
1046 (KS) for 2 and 24 h, respectively.

1047 (D-E) Same as in A-B, but for the area (D) and density (E) of postsynaptic gephyrin puncta.
1048 In E, Two-way ANOVA analysis showed a significant effect of time ($p = 0.04$) and interaction
1049 between treatment and time (§, $p = 0.04$).

1050 (F) Same as in I, but for normalized gephyrin density. $p = 0.047$ and 0.33 (KS) for 2 and
1051 24 h, respectively.

1052 (H) Same as A, but for normalized density of inhibitory synapses.

1053 Data are represented as mean \pm SEM. Data from 15 control images (N=3) and 15 LatB images
1054 (N=3) per time point.

1055

1056 **Figure 8. Inhibitory bouton stabilization by Sema4D requires MET.**

1057 (A) Time-lapse two-photon images of GAD65-GFP-labeled axons in organotypic
1058 hippocampal slices during wash-in (grey box) of combination of 1 nM Sema4D and DMSO
1059 (S4D; upper panel) or combination of 1 nM Sema4D with 1 μ M PHA-665752 (S4D+PHA;
1060 bottom panel). Only every second image is shown for clarity. Persistent and non-persistent
1061 boutons are indicated as in Figure 2. Images are maximum intensity projections of 15-16 z
1062 stacks. Scale bar 5 μ m.

1063 (B) Density of non-persistent boutons in slices treated with DMSO (C) and 1 μ M PHA-
1064 665752 (PHA): N – new (MW, $p = 0.28$); L – lost (MW, $p = 0.77$); S – stabilizing (MW, $p =$
1065 0.98); D – destabilizing (MW, $p = 0.24$); T – transient (MW, $p = 0.67$).

1066 (C) Fraction of non-persistent (NP) boutons in S4D- and S4D+PHA-treated axons: N:
1067 MW, $p = 0.34$; L: MW, $p = 0.74$; S: MW, $p = 0.01$; D: MW, $p = 0.64$; T: MW, $p = 0.53$.
1068 (D) Density of stabilizing boutons in slices treated with S4D or S4D+PHA (MW, $p =$
1069 0.006). Dotted line represents control values.
1070 (E) Frequency distribution of the stabilizing bouton density in S4D- and S4D+PHA-
1071 treated slices (χ^2 , $p = 0.048$).
1072 (F) Representative images of hippocampal slices treated with S4D (upper panel) or
1073 S4D+PHA (bottom panel) for 100', and stained for presynaptic VGAT. Images are average
1074 intensity projections of 5 z stacks. Scale bar 5 μm .
1075 (G) Normalized mean staining intensity for VGAT in S4D- and S4D+PHA-treated slices
1076 (MW, $p = 0.009$). Control value is indicated with dotted line.
1077 (H) Cumulative distribution of inter-event interval (IEI) of mIPSCs from CA1 pyramidal
1078 cells in organotypic slices after treatment with 1 nM Fc/DMSO (C), 1 nM S4D/DMSO (S4D)
1079 or 1nM S4D/1 μM PHA-665752 (S4D+PHA) for 24 h. C and S4D as in Figure 3K.
1080 (I) Fraction of non-persistent boutons in axons treated with MQ (control) or 10 μM Y-
1081 27632 (ROCK inhibitor): N: MW, $p = 0.05$; L: MW, $p = 0.39$; S: MW, $p = 0.02$; D: MW, $p =$
1082 0.38 ; T: MW, $p = 0.78$.
1083 Data are represented as mean \pm SEM. Data in B from 18 control axons (N=4) and 18 PHA-
1084 treated axons (N=4), in C-E from 17 S4D-treated axons (N=4) and 16 S4D+PHA-treated
1085 axons (N=4), in F-G from 16 images of S4D-treated slices (N=3) and 23 images of
1086 S4D+PHA-treated slices (N=4); in H from 14 control cells (N=5), 14 S4D-treated cells (N=7)
1087 and 17 S4D+PHA-treated cells (N=5), and in I from 21 control axons (N=5) and 22 Y-27632-
1088 treated axons (N=5).

1089

1090 **Figure 9. MET is enriched in a subset of inhibitory presynaptic boutons.**

1091 (A) Images of primary cultures of hippocampal neurons immunostained with MET
1092 nanobody (red) and markers for excitatory synapses: presynaptic vesicular glutamate
1093 transporter (VGLUT; green) and postsynaptic Homer (blue). The majority of MET puncta co-
1094 localize with one or both markers (white arrows), but some MET puncta do not co-localize
1095 (red arrows). Images are maximum intensity projections of 13 stacks. Scale bar 5 μm
1096 (overview) and 2 μm (zoom).
1097 (B) Same as A, but neurons were stained with MET nanobody (red) and markers for
1098 excitatory presynapses (VGLUT; green) and inhibitory presynapses (vesicular GABA
1099 transporter VGAT; blue). White arrows indicate MET co-localizing with VGLUT and blue

1100 arrows indicate MET co-localizing with VGAT. Images are maximum intensity projections of
1101 12 stacks. Scale bar 5 μm (overview) and 2 μm (zoom).

1102 **(C)** Same as A, but hippocampal neurons were stained with MET antibody (red) and
1103 VGAT (blue). Blue arrows highlight MET puncta co-localizing with VGAT, while red arrows
1104 indicate MET puncta that do not co-localize with VGAT. Images are maximum intensity
1105 projections of 17-21 stacks. Scale bar 10 μm (overview) and 2 μm (zoom).

1106 **(D)** Representative images of GFP-labeled inhibitory boutons (green) in hippocampal
1107 slices, stained with a nanobody (upper) and an antibody (lower panels) against MET
1108 (magenta). Images are maximum intensity projections of 5-6 z stacks. White arrows indicate
1109 MET enrichment in GFP-labeled boutons. Scale bar 5 μm .

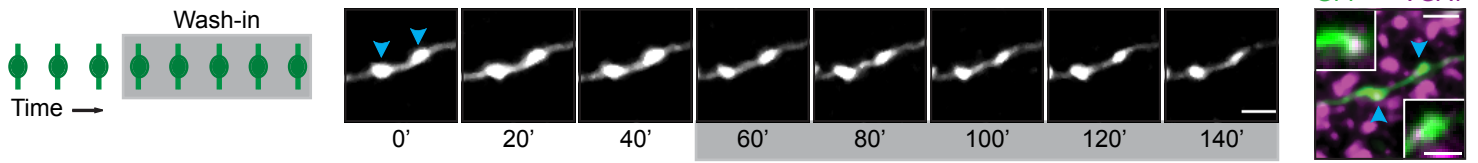
1110 **(E)** Fraction of GFP boutons positive for MET. Aspecific staining was determined by anti-
1111 myc staining without nanobody ('C'; black) and random co-localization was determined by
1112 inverting the MET channel ('Inv'; light gray) (Nanobody: KW, $p = 0.002$; Antibody: MW, p
1113 < 0.0001).

1114 **(F)** Example of two inhibitory boutons (green) in hippocampal slices showing enrichment
1115 in MET (magenta), and the respective xz and yz projections. Images are maximum intensity
1116 projections of 6 z stacks. Scale bar 1 μm .

1117 Data are represented as mean \pm SEM. Data in F from 10 control images (N=2), 12 images in
1118 MET and inverted group (N=3) for the nanobody staining and 15 images in MET and inverted
1119 group (N=3) for the antibody staining.

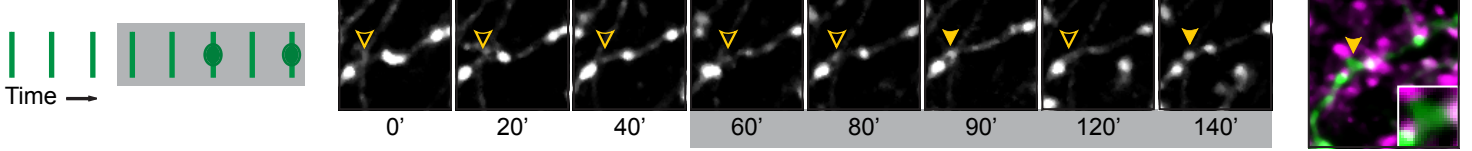
1120

A Persistent (P; ▶)

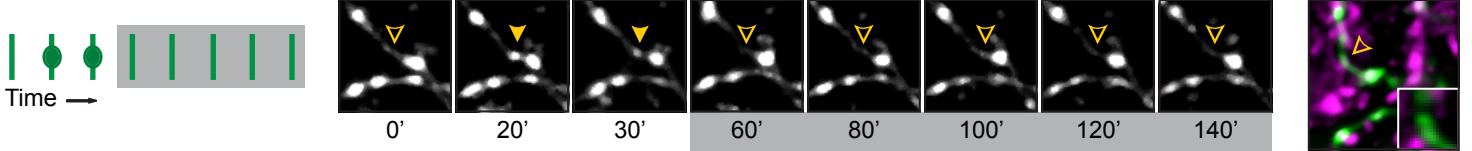


B Non-persistent (NP; present - ▶ - or absent - ▶ -)

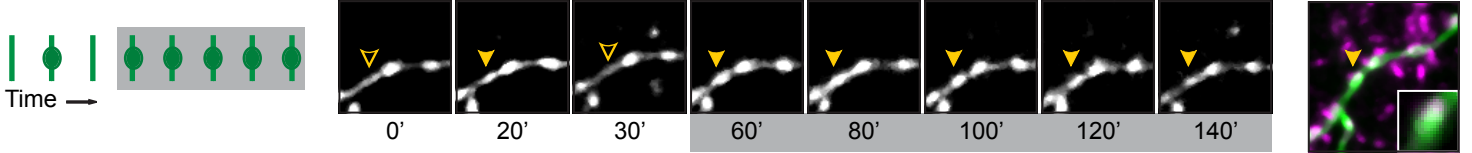
1. New (N)



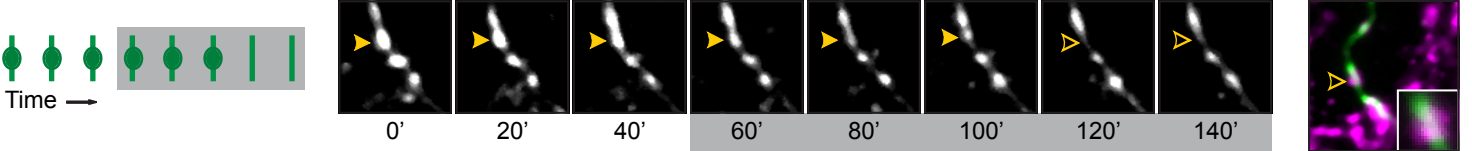
2. Lost (L)



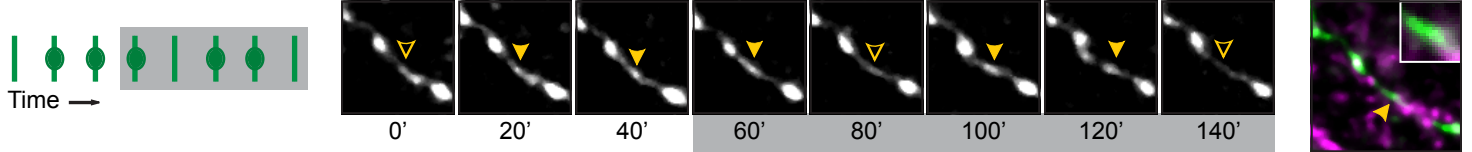
3. Stabilizing (S)



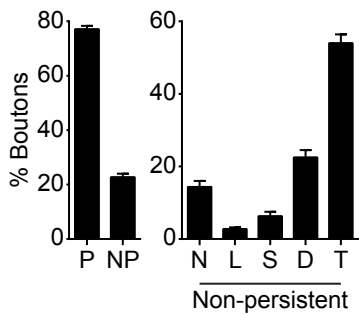
4. Destabilizing (D)



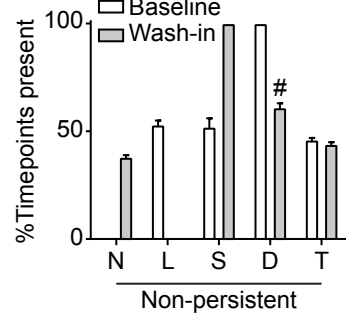
5. Transient (T)



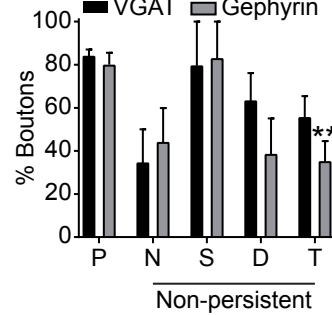
C



D



E



F

